FUDMA Journal of Renewable and Atomic Energy (FJoRAE)
ISSN: 3027-2335
Vol. 2 No June 2025. Pp 85-105

https://doi.org/10.33003/fjorae.2025.0201.06

Geo-Investigation for Gold Mineralisation Veins in Part of Kushaka Schist Belts, Niger State Nigeria, using an integrated approach

Adebayo, Abbass ADETONA[1]., Kazeem Adeyinka SALAKO[1]., Oyeleke Ismail OLARINOYE[2]., Adekola Amos ALABI[3]., Abdulwaheed Adewuyi RAFIU[1]., Usman Dafyan ALHASSAN[1]
[1] Department of Geophysics, Federal University of Technology, Minna, Niger State, Nigeria
[2]Department of physics, Federal University of Technology, Minna, Niger State, Nigeria
[3]Department of Geology, Federal University of Technology, Minna, Niger State, Nigeria
Correspondence: adetonaabbass@futminna.edu.ng ,E-mail/Mobile: a.abbass@futminna.edu.ng, 08036915982. ORCID: 0000-0002-3161-086X.
s.kazeem@futminna.edu.ng ORCID: 0000-0003-4016-4811
iyiolarafiu@futminna.edu.ng ORCID: 0000-0003-2434-4919
leke.olarinoye@futminna.edu.ng ORCID: 0000-0002-3433-5250
alabiadekola@futminna.edu.ng ORCID: 0009-0003-7662-3271

Abstract
The research attempt to delineate the exact position and depth to gold loads within sheets 164_Minna on latitude 9.30' to 10.00 North and longitude 6.30' to 7.00 East at the terminal end of Minna-Kushaka schist belt. The research employed magnetic, radiometric and very low frequency methods. Eight structural lineaments labelled F1 to F8 where mapped from magnetic data, these structures resulted from the deformation of the basement metamorphic rocks when intrude by volcanic intrusions. Majority of these faultiness area trending in the NE-SW direction. The Hydrothermal altered zones was investigated using K/eTh ratio, K_deviation and F_parameter derived from the Radiometric data, Regions with values Potasium-ratio_Thorium (K/Th) ranging from 0.3 – 0.5 %/ppm, K_deviation from 7.3 to 60.6 and F_Parameter from 0.8 to 1.3 respectively were delineated as having being considerably altered. A comprehensive analysis of these results, was used to produce a ternary image in which the delineated region of hydrothermal altered zones appearing in whitish and grey colour located around Minna and Tudun-Fulani, Shakwatu, Shekwata, Gunnu, Sarkin-Pawa, Shiroro, Gunni and Fuka villages. Euler analysis determine the of depths deposits ranging from 5 to 88 metres. Coincidentally mining activities are currently in progress around Shakwatu, Shekwata, Asha, Sarkin- Pawa which falls within the regions delineated. In view of the above, the study recommends the exploration for gold mineral along the profiles VLF A, VLF B, VLF C, VLF D, VLF E, VLF F, VLF G, VLF H, VLF I, VLF J and VLF K respectively. The highest hydrothermal signature correlates with biotite gneiss zones intruded by quartz schist, typical hosts for orogenic gold. The research indicated that location of potentials correlate to the region where exploration is currently going on and beyond, findings from this study can support safer and more efficient resource extraction with minimal environmental impact.
Key words: Hydrothermal zones, F-Parameter, K-deviation, Minna-Kushaka Schist belt

1.0 INTRODUCTION

A geologic classification of gold deposits according to the structural control of mineralisation was proposed by Roberts et al. (2005). One of these classifications is the Batholith Associated Quartz Vein deposits. This type of deposit consists of vein of quarts that have filled faulted openings resulting from brittle and or ductile deformation of metamorphic basement rocks. These deposits are often controlled by regional faults hosted within medium to high grade schists. (Roberts *et al.,* 2005)

Primary gold mineralization has prominent occurrence within the schist belt of northwestern and southwestern Nigeria, specifically in areas such as Anka, Kushaka, Birnin-Yauri, Birnin-Gwari, and Ife-Ilesha, to mention a few (Garba, 2003; MMSD, 2010). The quartz veins of the Precambrian age serve as the primary host rock within the country. (Adeleke et al. 2014).

[1] Corresponding Author's e-mail adetonaabbass@futminna.edu.ng; a.abbass@futminna.edu.ng

The distinct belts were identified within the study area as the Birnin-Gwari, Kushaka, and Ushami schist formations (Ajibade and Wright 1989). These are occupied by medium- to low-grade meta-sediments and volcanic rocks with poly-deformation. The intrusion of quartz veins and schist rocks could create alteration driven by hydrothermally altered zones (Bierlein et al. 1998; Yannah et al. 2015). These altered zones can be identified as narrow zones lying adjacent to the veins. It has two distinct zones, in which the first zone is light in colour at the side of the host rock and the second zone is a dark band adjacent to the vein intrusion (Jambon 2007).

Some of the major challenge facing the mining activities in this region is the devastation done to farm land by the crude method employed by artisanal miners. Secondly poor yield of exploration when the structures are at a greater depth, the miners usually abandon the mine in fear of collapse of the pits. The present research intended to mitigate this challenge by identifying the actual position of the structures hosting the ores and equally determine the depth to these ores. This research intends to address these challenges through the following objectives

i. Mapped the geological structures veins that serve as host to the targeted minerals from First Vertical, Horizontal Derivatives of Anomalous Magnetic Field of the study area. Employ Euler-deconvolution to estimate the depth to these mineral ores.
ii. Delineate the regions of hydrothermal alterations using K_deviation, F_parameter and Potassium-ratio-thorium normalisation from the analysis of ^{238}U, ^{232}Th and ^{40}K concentration and their ratio maps.
iii. determine the level of mineralization and competency of the area from the analysis and interpretation of Very Low Frequency (VLF)

The integrated approach using Aeromagnetic radiometric and Very Low Frequency is an additional advantage to other works that has been carried out in this area.
The final part of this work utilises 2_D resistivity model for correlate the VLF and ground radiometric data to assess the dose rate and compare it with the NORM to ascertain the safety within the mining site, this aspect is not contained in this publication.

2.1 Location of the study area

The reconnaissance work covers the entire Minna sheets (164E), an area of 55 kilometre square and it is enclosed between latitudes 9°5´N – 10°00´N and longitudes 6°00 - 6°5´E part of Niger State, Nigeria. Minna is located between longitude 6°25´E and 6°45´E and latitude 9°24´N and 9°48´N, Figure 1, it occupies the central portion of the Nigerian basement complex. Major towns within the study area include Minna Shekwata, Shakwatu, Gunu, Kuta, Shiroro, Sarkin-Pawa and Kushaka. Major occupation within these areas is farming and animal husbandry, rainy season is between Aprils to October.

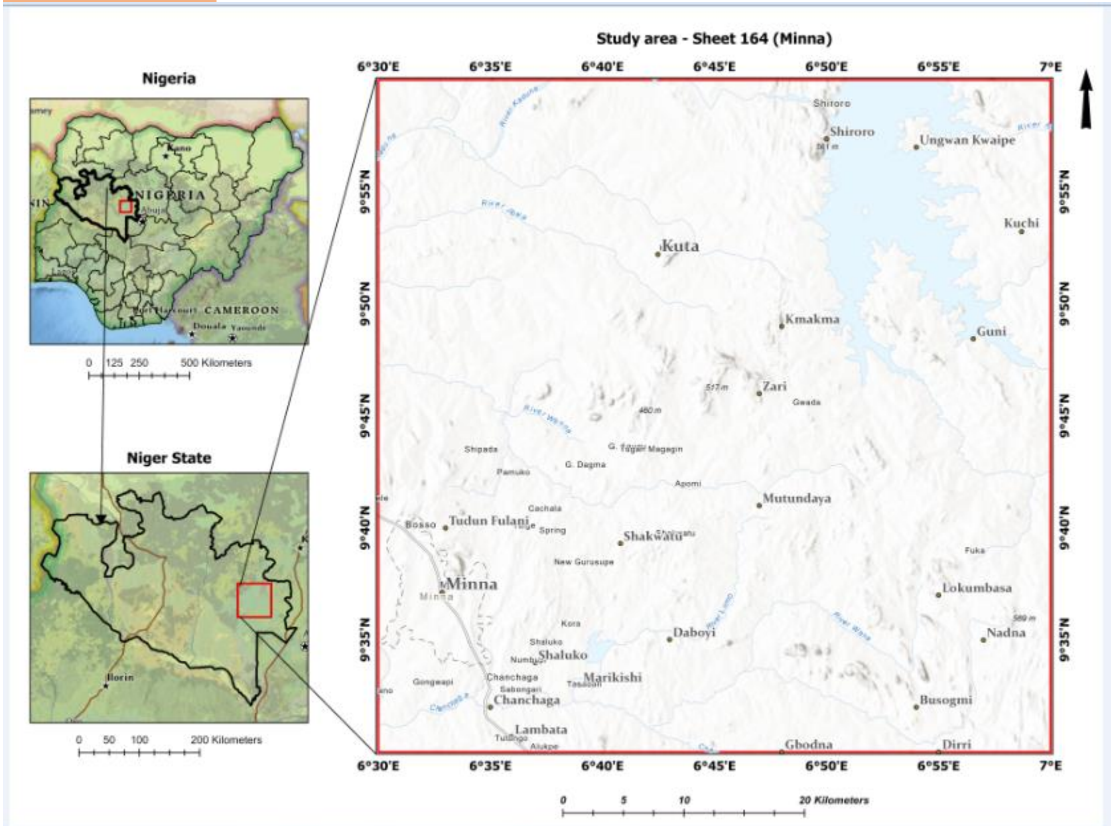

Fig. 1 Map of the study area

2.2 Brief Geology of the study area

This study area is geologically positioned around the igneous rocks of Northcentral Nigeria with isolated encroachment of the Nupe sedimentary rock at the North-eastern corner and Northern end (Fig 2). The area has meta-sediments which comprises of quartzites, schist, and phylites, and older granites consisting diorites, rhyolites that intruded into base rock gneisses, meta-sediments, and granite rocks of Anka-Yauri schist belt around Kebbi state (Danbatta 2008). The region consists of faulted zone of parallel phylites, deformed and pre-deformed quartzite that gave birth to the Anka trans-current fault zone that is classified as pan-Africa crustal suture (Danbatta 2005).

A little portion of the area of interest is occupied by sedimentary rocks that comprise sandstones, shale and limestone of the Nupe basin, the only sedimentary formation in the country that is directly underlain by basement rocks. The region occupied by the Nupe sand stone comprises of four lithologic units namely: siltstone, sandstone, shale, and limestone (Augie and Ologe 2020; Olugbenga 2020). The southern end of the Kebbi within the basement complex is classified as Zuru-Yauri schist belt. According to Danjumma et al. (2019), this zone of the schist belt comprises of muscovites-biotite banded gneisses, porphyroblastic gneisses, migmatites, schist, quartzites, metavolcanics (amphibolites), quartzites, mica schist, granulites, and older granites.

Major geological formations encountered within this belt have structurally dispositions in the NE-SW to NNE-SSW directions; a NW-SE trending fault line and a major N-S trending Zuru anticlinorium (Danbatta 2005; Sani et al. 2019). Composition of this schist varies in lithology from the other schist belts in the north-western Nigeria due to its predominant compositions of quartzites with very subordinate schist and amphibolites (Danbatta 2008; Danjumma et al. 2019).

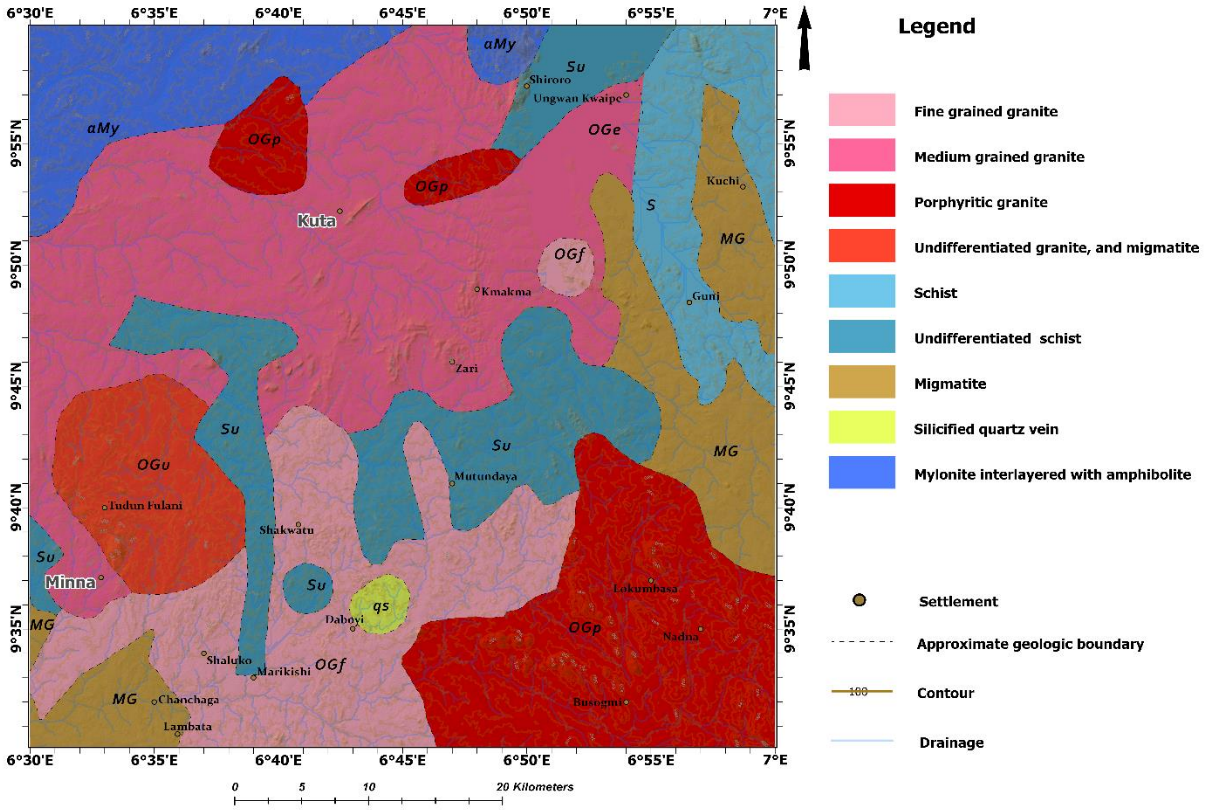

Fig. 2 Geology map of part of the Study area modified from Geology of Nigeria (NGSA)

3.0. MATERIALS AND METHOD

Aero-magnetic data covering Minna sheet 164 and the respective radiometric data consisting of Potassium, Thorium and Uranium, was obtained from Nigerian Geological Survey Agency (NGSA). Other materials include: Geology and Geographical location map of the study area, software such as Geosoft Oasis Montaj_version 9.0, ArcGIS_version 10.2, Google Earth, and Computer system.

Table 1: Parameters adopted during the survey (NGSA)

Survey Parameter	Magnetic Specifications	Radiometric Specifications
Data Acquired by:	Fugro Airborne Surveys	Fugro Airborne Surveys
Time Range	2005 – 2009	2005 – 2009
Data Recording Interval	0.1 seconds or less	0.1 seconds or less
Sensor Mean Terrain Clearance	80 meters	80 meters
Flight Line Spacing	500 meters	500 meters
Tie Line Spacing	5000 meters	2000 meters
Flight Line trend	135 degrees	135 degrees
Tie Line trend	45 degrees	45 degrees
Equipment: Aircraft	Cessna Caravan 208B ZS-FSA, Cessna Caravan 208 ZS-MSJ	Cessna Caravan 208B ZS-FSA Cessna Caravan 208 ZS-MSJ
Equipment:	3 x Scintrex CS3 Cesium Vapour Magnetometer	(NaI "TI" crystals) 512-channels gamma-ray spectrometer

Procedure:

Aero-magnetic data processing

The total magnetic intensity (TMI) data of the area of interest was subjected to various near surface enhancement and filtering techniques, among which are: regional residual separation, reduction to magnetic equator, first vertical derivative, Total Horizontal Derivative, and the 3-D Euler Deconvolution for depth estimation to magnetic structures.

a) Aero Radiometric data processing and interpretation

This research will map regions of hydrothermal alteration as a result of magmatic intrusions by employing the concept of eTh/K ratio, K_deviation and F_parameter from the radiometric data, and select regions that correlate with structural features such as faults, fracture, dykes, joints and foliations mapped from magnetic data analysis as zones of mineralisation.

The Aero radiometric data of the study area was employed primarily to delineate region of hydrothermal alteration. This was achieved through these procedure stages:

1. Computing the K/eTh ratio, a high value of K/eTh concentration is an indicator to altered zones.
2. Potassium-deviation (K_deviation) is obtained from employing the method developed by Saunders et al. (1987) and Pires, (1995) equation 5. A high value is an indicator of a hydrothermal altered zone.
3. Computing the F-parameter using equation 6 equally a high value of F_parameter indicated that the regions have undergone hydrothermal alteration.
4. Finally, a ternary image using the eTh/K ratio grid, K-deviation grid, and the F-parameter grid is produced for analysis of the regions of hydrothermal alteration.

3.1. Theory of Enhancement Techniques

First Vertical Derivative (1VD)

The vertical derivative of the field is intended to enhance the shallow features while attenuating the deep seated features. It sharpens the shorter wavelength at the shallow subsurface region, in the same vein observe the lateral variation of the susceptibility so as to map any sharp discontinuity within the field that could depict fracture or fault line. (Aliyu et al. 2021; Adetona et al. 2023). Computing the 1VD could be angle complex due to a simple fact that the study area lies within the equator where the angle of inclination is less than 15^0.

Note that at the equator, the vertical component of the magnetic field is Z = TCos θ

Where θ = 90^0 this implies that Z = 0 at the equator, therefore, to evaluate the vertical derivative of the data, it needs to be taken to an imaginary pole where θ = 0, where the magnetic intensity is maximum and the vertical derivative can be computed. Therefore, the 1VD was computed from the anomalous magnetic field reduced to equator and inverted (AMF-RTE-inverted).

3.1.1. Total Gradient Amplitude (TGA).

Total Gradient Amplitude (TGA) can be computed from the "root mean square" of the (squared sum of the vertical and orthogonal derivatives) of the anomalous magnetic field (Li 2006; Li and Nabighian 2015).

$$A\,(x, y) = \sqrt{\left(\left(\frac{\partial T}{\partial x}\right)^2 + \left(\frac{\partial T}{\partial y}\right)^2 + \left(\frac{\partial T}{\partial z}\right)^2\right)} \qquad (1)$$

Where A (x, y) constitute the amplitude of the total gradient of the signal at the (x, y) plane, T is the measured magnetic susceptibility, $\partial T/\partial z$, $\partial T/\partial y$, $\partial T/\partial x$ are the vertical and perpendicular derivatives along the z, y and x planes, respectively. (TGA) is devoid of ambient field and the direction of the source anomaly. A unique feature of this algorithm is in its ability to locate anomaly vertically above the source body through vector resolution of the effect of the angle of inclination and declination of the field data.

3.1.2. 3-D Euler Deconvolution Technique

The use of Euler Deconvolution algorithm is aimed at achieving two primary purposes; delineating structures such as contact, and its apparent depth. Due to its unique ability in performing regional residual filter to the source data, this enables the use of total field data and the versatile nature of the equation generated which can be filtered to obtain the desired result. Structural index of 1 was employed in generating the equations for this study area, adjustment were made to the channels dxy and peak values until an acceptable results that correlate with geology and other structures observed in the TGA was obtained (Thompson 1982; Reid et al. 1990)

The 3_D standard Euler deconvolution technique relies on solving Euler's homogeneity equation (3) (Reid et al. 1990):

$$(x - x^\circ)\frac{\partial T}{\partial x} + (y - y^\circ)\frac{\partial T}{\partial y} + (z - z^\circ)\frac{\partial T}{\partial z} = \eta(\beta - T) \qquad (2)$$

where β is the regional field value and x^0, y^0, z^0 defines the position of the anomaly, η is the SI, and important in identifying the structural geometry and depth. (Reid et al. 1990).

3.2. Hydrothermal alteration indicators

Primary gold mineralization is usually found in association with poly-deformed metamorphic rocks and the rocks within the area have undergone poly-phase deformation and metamorphism (Alabi 2010). The basement rocks of the north central Nigeria have also been intruded by granitic rocks. These intrusions are completely capable of driving the hydrothermal system at a temperature range of 100 to 500 °C (Cunha L O *et al* 2017) which are responsible for primary gold mineralization in quartz vein intrusions into basement rocks. (Airo, 2002; de Quadros et al. 2003; Cunha et al. 2017).

Due to the fact that thorium is geochemically immobile when compared with potassium and uranium, it is used for normalisation of the radiometric data due to lithology variations that is caused by environment weathering and lithology on K and eU concentration. Galbraith and Saunders (1983), Saunders et al. (1987), Adams and Pires (1995) showed that thorium impoverishment mostly occurs with potassium enrichment during hydrothermal alteration processes. This hydrothermal alteration syn-mineralization subsystem is normally associated with various types of volcanic-associated massive-sulfide (VMS) base-metal and gold deposits. (Dickson and Scott, 1997; Maden and Akaryali, 2015; Cunha et al. 2017; Sanusi and Amigun, 2020).

In order to specifically mark out regions that has undergone potassium enrichment, ratio of equivalent thorium concentration to the measured potassium counts i.e. eTh/K, the F_parameter, which is the ratio of the product of potassium (K) counts and equivalent uranium (eU) concentration to the equivalent of thorium (eTh) concentration, as proposed by Efmov (1978), and the deviation from the ideal K values (K_d) proposed by Saunders et al. (1987), were utilized in mapping hydrothermal alteration haloes that are related to orogenic gold mineralization in the study area. The analysis of each of these three analysis are computed separately.

The potassium Deviation (K_d) from the nominal K values which represent potassium enrichment values due to hydrothermal alteration processes is obtained from Eq. 7 de Quadros et al. (2003):

$$\boldsymbol{K_d} = \left(\frac{K-K_n}{K_n}\right) \qquad (3)$$

Where K_d represent the potassium Deviation, K is the measured field potassium concentration and K_n the nominal potassium value,

Employing the method develop by Saunders et al. (1987) and Pires (1995), the nominal K value (K_n) is obtain from the relation, (de Quadros et al. 2003):

$$\boldsymbol{K_n} = \left(\frac{K\ grid_{average}}{Th\ grid_{averaage}}\right) * \boldsymbol{Th\ map} \qquad (4)$$

Values of K grid average and Th grid average were generated from the statistics of individual databases of both radioelements concentration. A high K_diviation value is an indication of hydrothermal alteration. The F_Parameter which reflects two relevant concepts which are: abundance of K related to eTh/eU ratio and the affluence of eU related to the eTh/K ratio given is by equation 6 (de Quadros et al. 2003):

$$\boldsymbol{F} = \frac{K * eU}{eTh} = \frac{k}{\frac{eTh}{eU}} = \frac{eU}{\frac{eTh}{k}} \qquad (5)$$

These three ratios are computed separately and they produced similar results, any one of them can be employed for the subsequent analysis

The $\frac{eTh}{k}$ ratio is simply the inverse of the $\frac{k}{eTh}$ computed. The $\frac{eTh}{k}$ result when correlated with that from F_parameter and K_deviation analysis will show a low within regions of highs.

To have a holistic treatment of the three approaches, the integration of these results can be achieved by constructing a ternary image, in RGB (Red for K_deviation, Green for F_parameter, and Blue for K/eTh,). However, for an acceptable analysis, it is necessary that all the initial information is correlated in the same direction (positive anomalies are correlated), (An et al. 1991; Agterberg and Bonham-Carter, 1999; Quadros, 2000).

4.0 ANALYSIS RESULTS AND INTERPRETATION.

4.1.1 The Anomalous Magnetic Field

The anomalous magnetic field of the study area Fig. 3, depicts the magnetic intensity across the field when the regional geomagnetic field (RGF) of 33,000 nT was removed from the total magnetic intensity. The magnetic intensity values of the study area range from -119.7 to 1477.4 nT with majority of the field indicating positive anomaly at the upper northern end of the study area was generally observed. The upper part of the study area displayed a mixture of both low and high magnetic anomalies whole the lower part are mostly inhibited by high magnetic susceptibility. The contrasting variation in susceptibility of the area is a clear reflection the contrasting geology of the area and a high degree of deformation of mafic magnetic rocks such as migmatite, gnesis quartz schist, mica schist, porphyritic, and middle grain granite and dolerite.

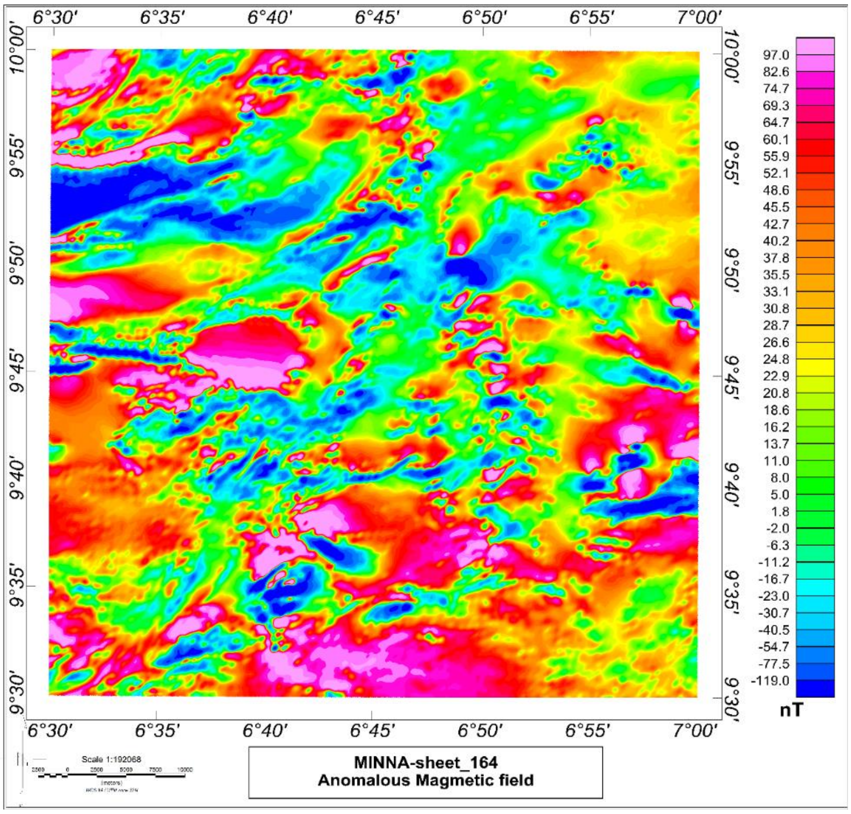

Fig. 3 Anomalous Magnetic Field Map

4.1.2. First Vertical Derivative

The result from the first vertical derivative of the Anomalous magnetic field that was computed in the frequency domain is quite revealing. Two distinct sections were observed based on the colour aggregate, the upper Northern end extending downward as a narrow band to the right and left of a triangular body at the southern end is marked by blue coloration. This is an indication of relatively average magnetic intensity values within an evenly undisturbed magnetic rock. Rock types identified with these region from the geology map in Fig. 4, are sandstone, amphibolites and mica schist. Two similar regions: (1) the western end down to the south western corner, (2) a pyramid-like structure at the southern end and the Eastern flank are all marked by a mixture of high (pink) and low (blue) magnetic signatures. Total amplitude gradient for these regions can be interpreted as regions of high frequency magnetic signatures of near surface basement rocks that has undergone high level of deformation.

Rock types that dominate these regions include Biotite gneiss, granite gneiss, prophyritic granite and Quartz schist. These regions depict distortions to the magnetic signatures but within these distortions a careful observation reveals some orderly linear structures that could be interpreted as lineaments that infer fractures, faults and joints. These lineaments are mapped and labelled F1 to F8. Majority of these lineaments cut across various lithology while some are at the boundary of different lithology among which are F9, F6, and F2. F8 is a noteworthy fault lines that cuts the study area into two sections diagonally, passing the boundary of rocks such as granite migmatite and gneiss. Also worthy of note are structures in red that could be found at different location on the field which is interpreted as dykes. The combination of these structures is the features that control the mineralisation pattern of the study area.

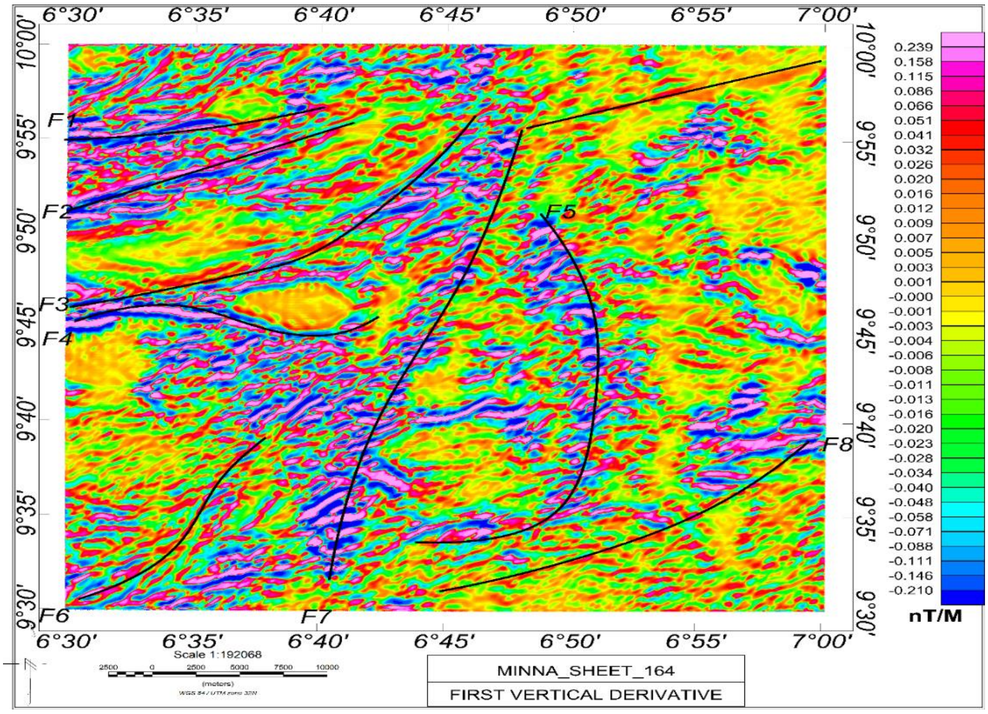

Fig. 4 First Vertical Derivative Map for the study area

4.1.3. Euler Deconvolution

Euler deconvolution was computed using the structural index for dyke (1) and sphere (2), the resulting data table was filter using the depth and dxy channels to an acceptable values in which the depth estimates from Euler deconvolution are accurate within ±10 meters, using a window size of ¼ of the sampling interval. Majority of the high density structures detected were located at various part of the field and at varying depths (Fig. 6). Major regional trends are in the direction of NE-SW and NW-SE. The depth of these structures are in the range 0 to 5 meters in the majority and are found within the Zungeru axis, followed by those at the depth range from 5 to 86 meters deep. Structures with greater depths are situated at above 50 meters at the South East and South western part of the study area.

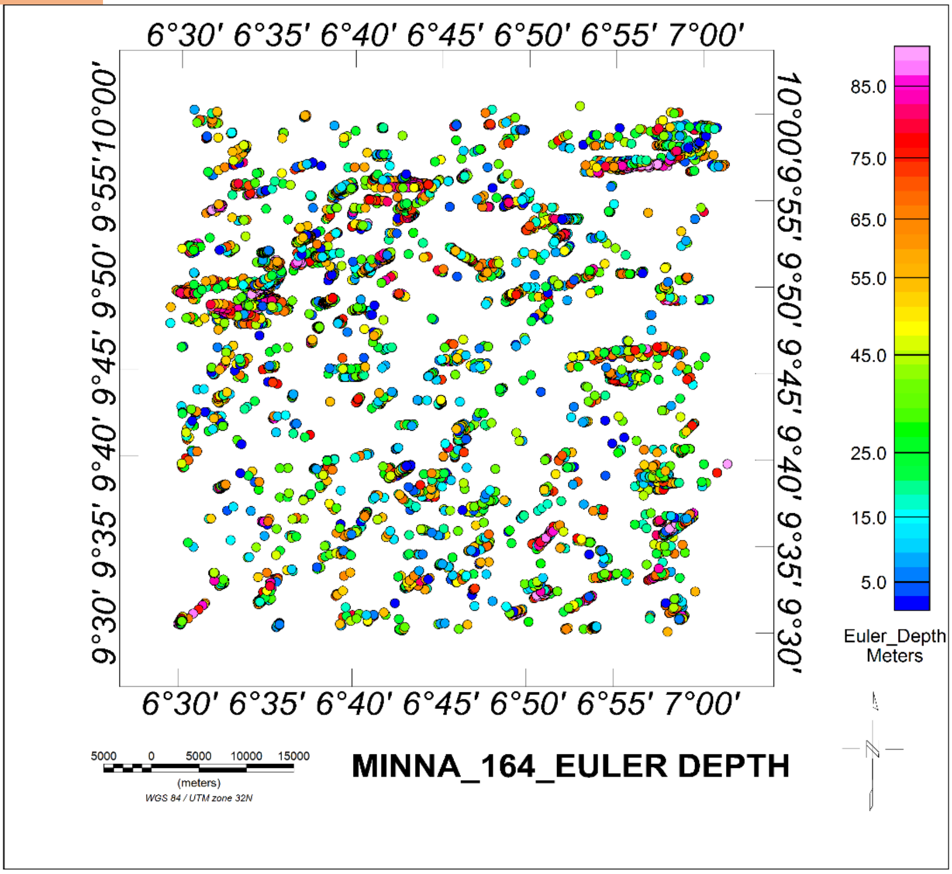

Fig. 5 Euler Deconvolution Map for detected Structures and respective depths

4.2.0 Result of Analysis of Radiometric Data
Each of the radiometric elements was "normalized" as follow:

$normK = K/(K+Th+U)$
$normTh = Th/(K+Th+U)$
$normU = U/(K+Th+U)$

This is intended to correct for attenuations that may occur do to the effects of water bodies and vegetation on the field the resultant radiometric anomalies are reliable to within 90% confidence based on spectral noise thresholds in mapping geological features and structures.

4.2.1 Concentration of K
Potassium is readily present in igneous rocks that are the major lithology across the field. This is evident in its abundance where its maximum concentration is noticed, majorly at the South-eastern and Western end of the study area, where fine grain granite and porphyritic granite intruded into the in-situ rocks.

4.2.2 Thorium concentration
The Thorium concentration in the study area varies from 0.76 to 20.97 ppm with maximum concentration covers the Eastern part of the area
4.2.3 Uranium concentration
Similar feature appears for Uranium concentration, though its concentration varies from 0.30 to 4.07 ppm highest at the North-Eastern corner, is sandwiched by a very low concentration with high concentration appear at the middle down to the southern end of the area
The low concentration for these three elements can be associated to the attenuation in concentration due to the presence of body of water within the reservoir. This effect was normalized by using thorium which is generally immobile. variation in the lithology as a

result of vegetation cover or water bodies was normalized as seen on K/eTh, K/eU and eTh/k ratio maps

As eTh is immobile compared to U and K, it is utilized as a lithological background control that defines ideal K value and concentration of eU in identification of hydrothermally altered haloes. Thus, eTh values are needed to conquer effect of lithology on K and eU concentration. (Saunders et al. 1987)
Felsic rocks are light, composed of light colour minerals rich in silica content, poor in magnesium. Mafic rocks are dark in colour, rich in magnesium, and poor in silica.
The South-Eastern corners of the study area that host the Bida sandstone with medium concentration on the K concentration map are converted to low concentration on the K/eTh ratio map. Similar observations were observed on the K/eU ratio map, where the deep sited low K concentration has been normalized.

4.2.4 K-deviation, K/Th ratio and F-parameter maps.

The potassium deviation maps were obtained for K/eTh, K_deviation (from equation 5) and F_parameter (from equation 6) respectively these three results are the required information to targeted regions of hydrothermal alteration. Targets are anomalous high K-deviation and F-parameter coinciding with anomalous high K/eTh that falls within regions of identified magnetic structures which imperatively are the signatures that characterized regions of orogenic gold deposits (Sanusi and Amigun 2020a; Saunders et al. 1987; Maden and Akaryali 2015).
The K/eTh ratio, K-deviation and F-parameter (Fig. 7, 8 and 9), these three results were simultaneously interpreted due to the correlation observed in their result. On the K/eTh ratio map Fig. 7, an anomalous high concentration is observed within those main blocks which are the entire North-Eastern corner and part of the Southern end. Similarly, the K-deviation result shows high concentration at the North Eastern corner of the study area and several loose of isolated highs at the North-western portion down to the Southern end of the study area, these are signatures of an accentuated potassium enriched haloes relating to gold mineralization. The F-parameter result on Fig. 9 has high concentration within the similar locations on the study area. These areas are located at the North-East around**, Shakwatu, Shekwata, Asha, Sarkin- Pawa** villages, which are hosted by various grades of granite migmatite and schist equally at the North-Western region of the study areas, where Quartz schist intrude into Biotite Granite and Granite Gneiss is intruded by Quartz schist and dolerite and at the lower end where Amphibolite schists, undifferentiated schist and granite Gneiss interlocked.

4.2.5 Ternary Image

The ternary image produced by combining the results from the three analysis K/eTh (in Blue), K-derivative (in Red) and F-parameter (in Green) as shown in Fig. 10 depicts area of anomalous high hydrothermal altered haloes in white colour and moderate altered hydrothermal haloes in (grey-blue) colour. These are areas are to the Western region, the South East corner and the some few points at the North Eastern area, which falls within Maikunkele, Shakwatu, Shekwata, Kafin-Koro and Sarkin-Pawa axis. These regions are intruded by fault-lines labelled F1, F2, F3, F4, and F5 respectively. Those altered zones delineated at the Southern end of the study area are influenced by fault-lines labelled F6, F7, and F8 respectively.

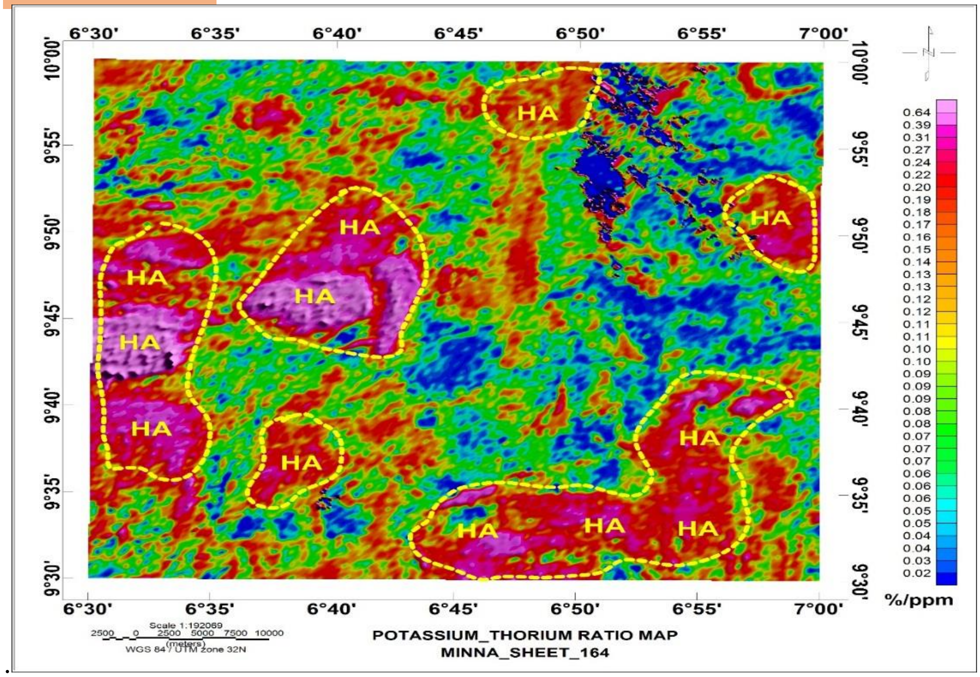

Fig. 6 Potassium_Thorium ratio map

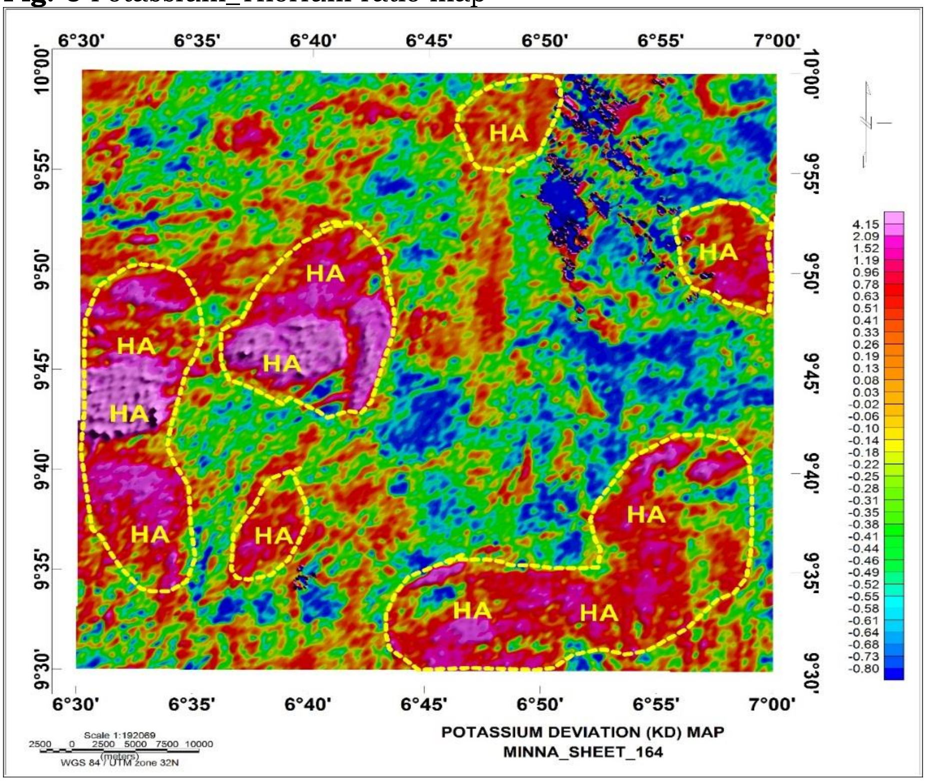

Fig. 7 Potassium Deviation Map

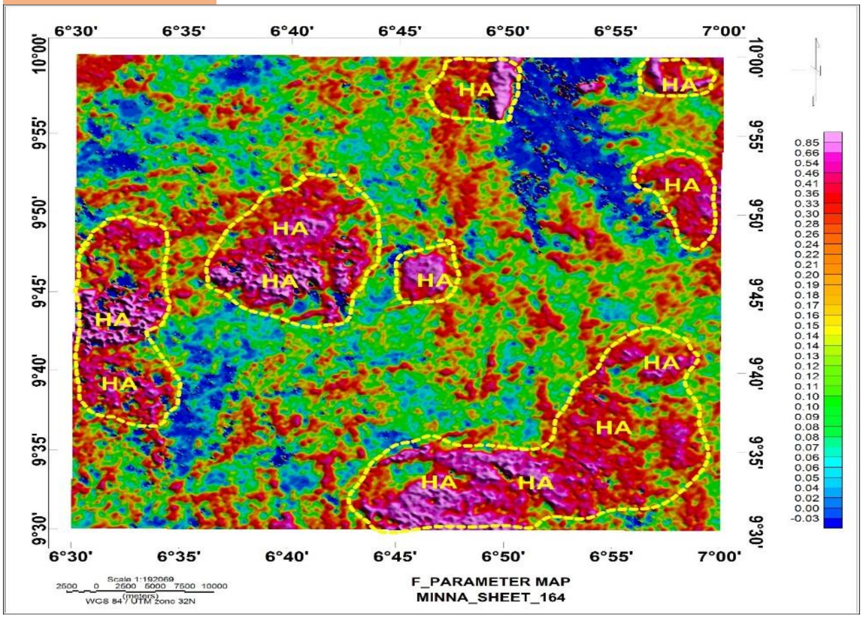

Fig. 8 F_parameter Map

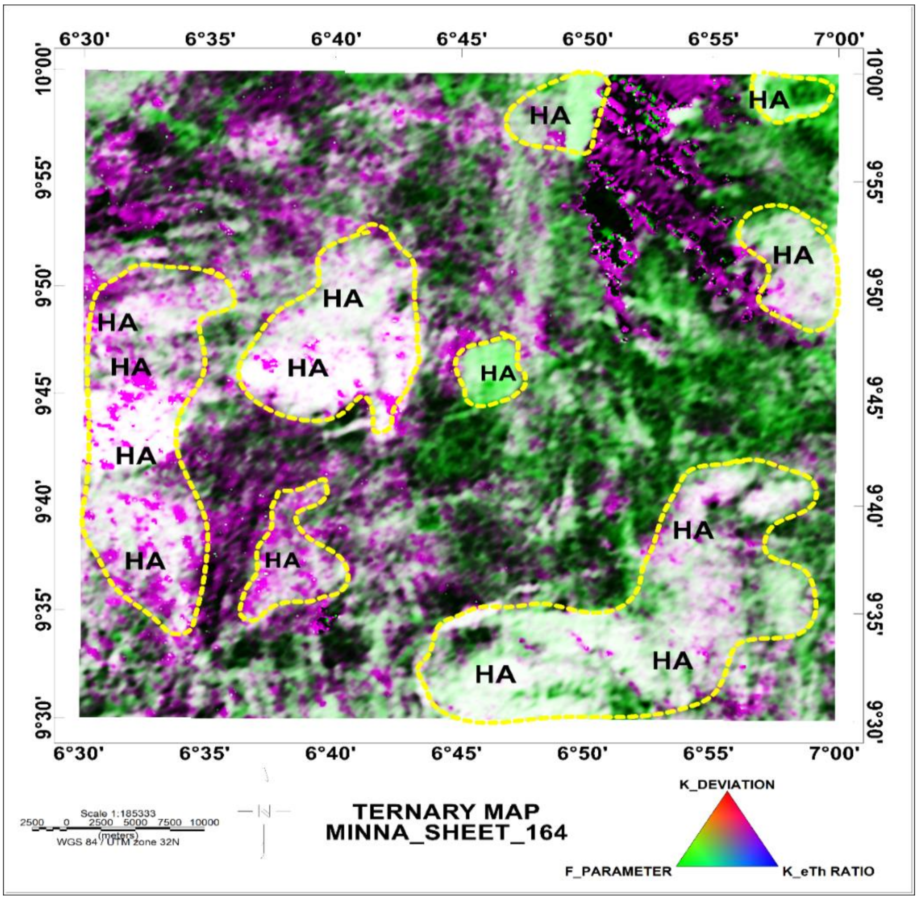

Fig. 9 Ternary Image produced from combination of results from K_deviation, Potassium_Thorium ratio and F_parameter

A total of Five (5) survey profiles with Northwest- Southeast orientations having inter-profile distances of 200 meters and inter-station spacing of 20 meters along each profile were generated across the strike formations, hence a total of 156 VLF stations were established, and from which VLF data was generated from each point of interest. This inter-profile and inter-station spacing is sufficient to give a very high density of data that will reveal high resolution subsurface geological image of the area.

The Scrintrex Envi VLF Instrument was deployed in this investigation and oriented along the frequency transmitter, and a frequency of 21.1 kHz signal with callsign RDL from Russia having the best signal strength was selected. VLF data was then collected at the established stations which are along the dip direction (along profiles) of the rock outcrops in order to reveal the lithologic variations, (because lithologic variations occur along the dip direction and the dip direction is perpendicular to the strike).

The data acquired from the VLF survey was then analysed and qualitatively interpreted using MICROSOFT EXCEL, KHFFILT and OASIS MONTAJ software.

The interpreted VLF data yielded areas with high and low conductivity with potentials of mineralisation, as such, points on the profiles indicating high and significantly low conductivity were mapped out, and 12 VES points were established to estimate depth to conductive bodies on the profiles.

VLF Interpretation along Profile A

At location VLF A with traverse oriented in the W-E direction, a plot of filtered data shows a prominent positive response between 700 m and 800 m (Figure 10) along the profile resulting in probable fracture zone or presence of conductive subsurface structure located between 700 and 800 m at the depth extending from 0 m to 60 m. There are other positive responses along the profile such as at points 220 and 280 m, 440 and 500 m, 1120 and 1250 m resulting in not well-fractured zone, they could be an inflection points without any geological implication. While prominent negative response between 850 m and 900 m resulting in probable high resistive formation located between 850 and 900 m along the profile at the depth between 30 m and 60 m, this point is also not competent for engineering work, because a thick over burden.

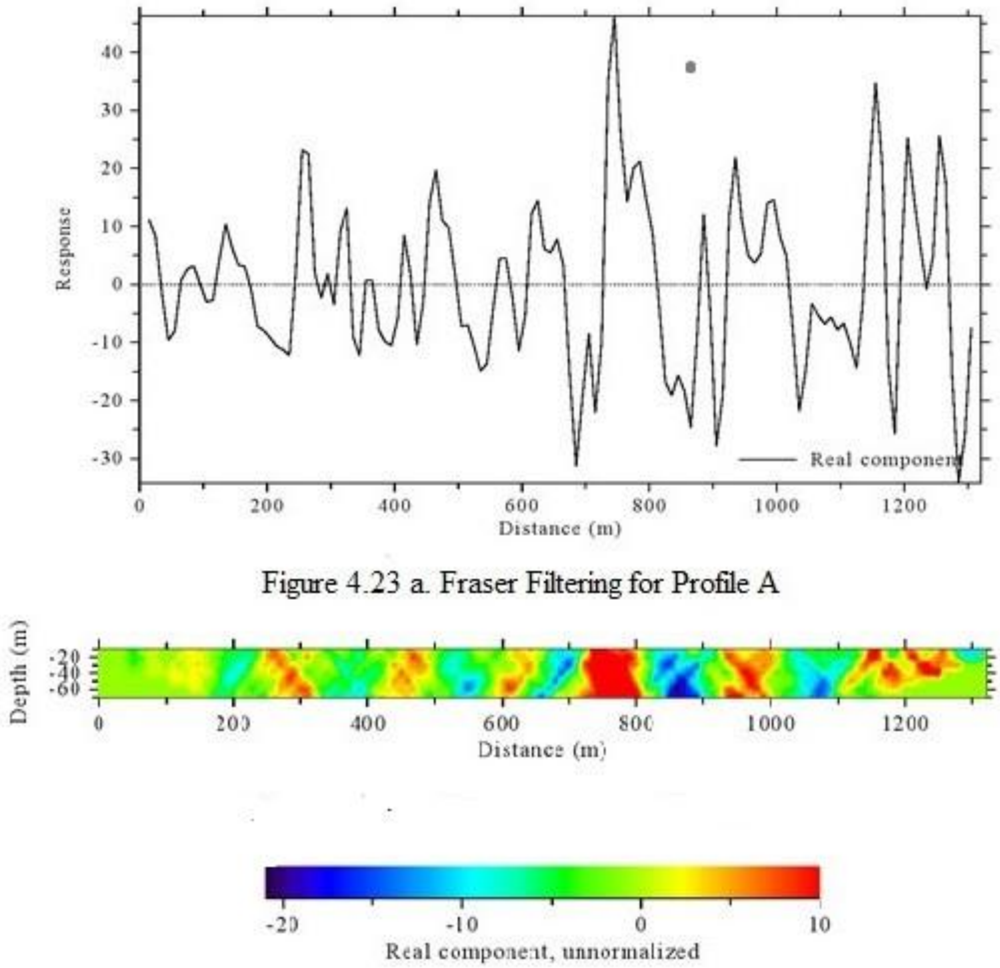

Figure 10: Karous-Hjelt filter for profile A

VLF Interpretation Along Profile B

At location VLF B with traverse oriented in the W-E direction, a plot of filtered data shows seven (7) distinct zones of positive peaks (high conductivity) these zones ranges between 50 and 100 m, 200 and 300 m, 400 and 500 m, 580 and 680 m, 780 and 820 m, 900 and 970 m, and 1100 and 1220 m (Figure 11). The first, third, fifth and seventh zones could be an inflection points without any geological implication. However, the second, fourth and sixth on the transverse B showed a conductive response greater than the previous zones.

Similar results are available for profile D, E, and F a summary and interpretation for the six profiles can be seen on figure 13.

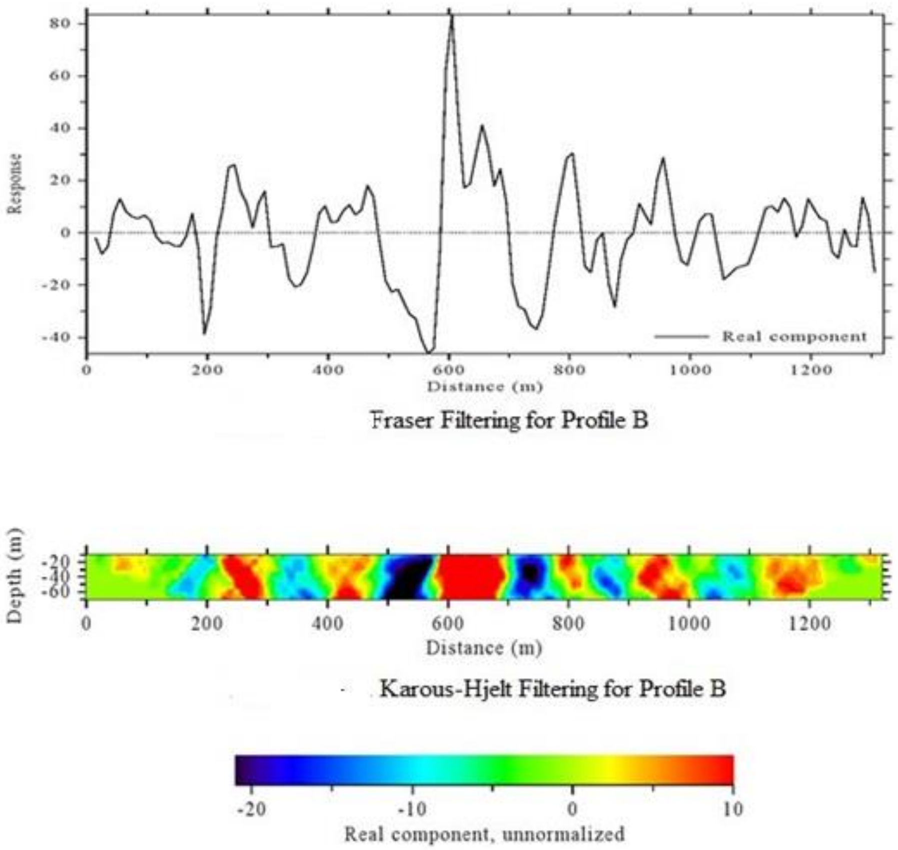

Figure 11: Karous-Hjelt filter for profile B

At location VLF C with traverse oriented in the W-E direction, a plot of filtered data shows six (6) distinct zones of positive peaks (high conductivity) these zones ranges between a prominent positive The third, fourth, fifth and sixth zones, between (780 and 800 m, 900 and 1000 m, 1090 and 1120 m and 1240 and 1260m) could be an inflection points without any geological implication. However, the first and second zones on the transverse C showed a conductive response greater than the previous zones.

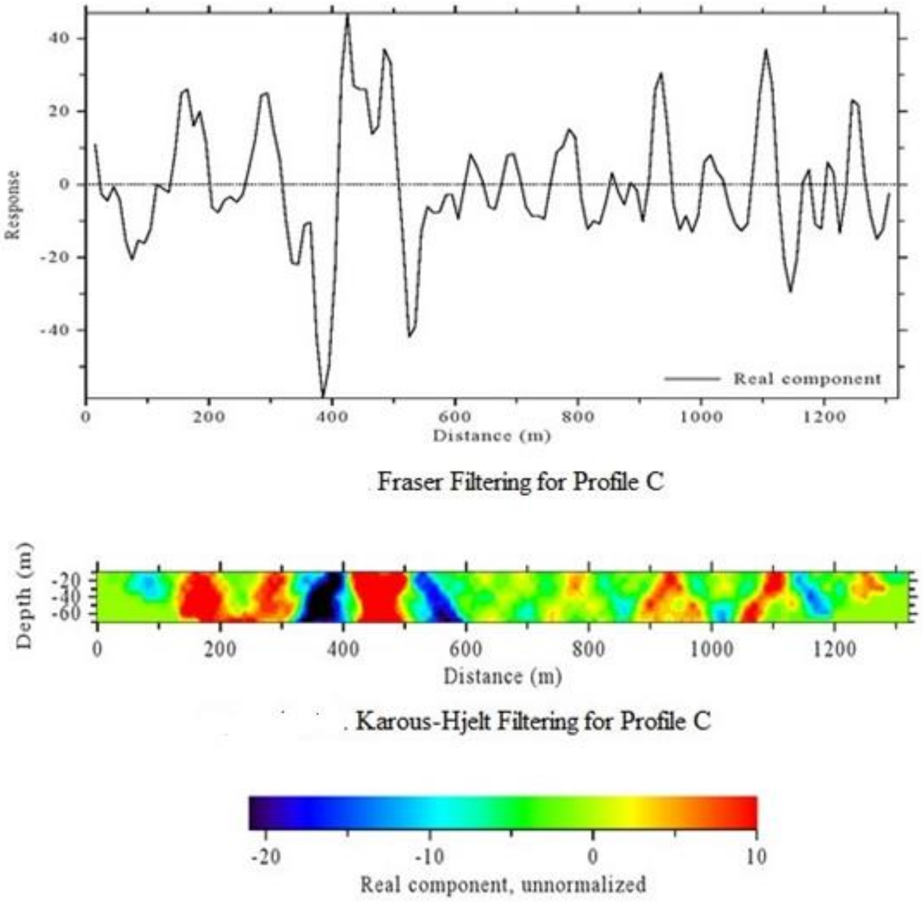

Figure 12: Karous-Hjelt filter for profile C

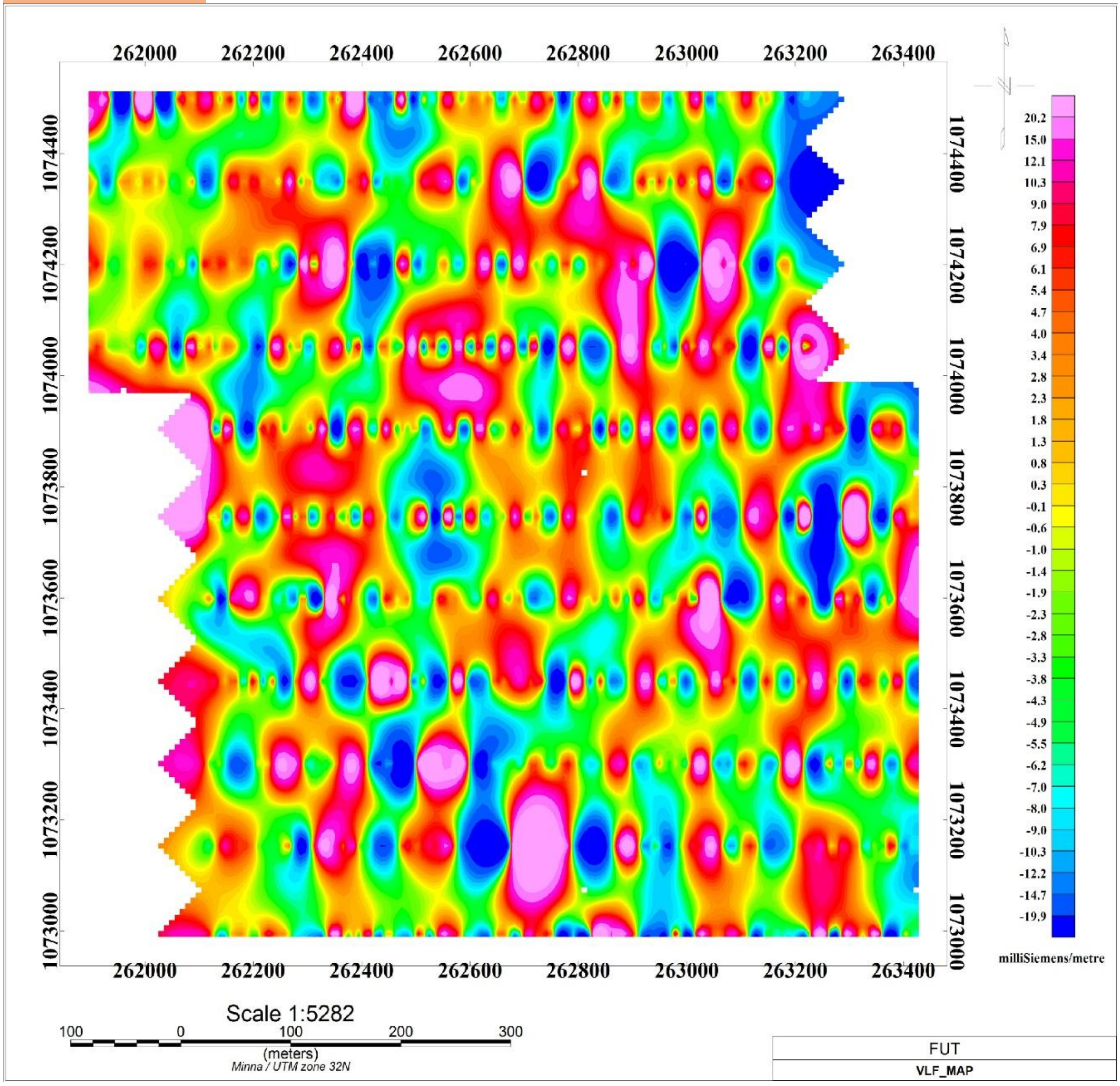

Figure 13: Karous-Hjelt filter for across six profile on the field

4.2.6 Summary and Interpretation of result

The major fault line delineated within the study area are generally within the regions where the major basement rocks were intruded by other minor lithology such as quartz dolorite mica etc. Majority of these structures trend in the NE – SW directions, few in N – S direction which is a result of the structural deformation resulting from relief from stress generated during the separation of South American plate from African plate, coupled with the tectonic deformation within the region. The structural trend within the area agrees with the established trend along the Ifewara to Zungeru Faultline that runs through the country. These faulting systems defines the Late Pan African ductile deformation (2530 Ma) that hosts gold mineralization in the Kushaka, and Auna schist belt (Garba, 2000; Sanusi and Amigun, 2020b).

The beads like shape multicolour that is observed on the structure displayed on the Euler map reflects variation in location cum depths levels of the observed source bodies (dyke contacts on joints) With a structural index of 1 which is targeted for dykes and a window size of ¼ of the sampling interval of Fig. 6 the Euler analysis predicted a depth of 5 to 86 meters for most of the structures delineated on the field.

Comparing the concentration of the elements Potassium, Thorium and Uranium with the normalised ratio maps of K/Th, K/Th indicates clearly the role of normalisation of the concentrations using Thorium by attenuating effect of lithology variations due to vegetation, water body and other contrasting lithological variations. This is clearly illustrated on the K/Th map (Fig. 7). Notably, high K/Th, F-parameter, and Kd values are suggestive of hydrothermally altered zones that are enhanced by potassium enrichment (Akinlalu 2023; Sanusi and Amigun 2020a; Eleraki et al. 2017; Abd El Nabi 2012).

The ternary map from K/Th, K-deviation and F-parameter show that the regions occupied by sandstone appears black, indicating the result of low concentration of potassium within the Amphibolite Schists. The four outcome maps: location, geology, structural and hydrothermal maps were superimposed on each other to produce Fig. 11 which interprets the faults zones, the rock type and location of hydrothermal alteration that are possible location of haloes of orogenic gold mineralization. Locations that fall between the very high to moderate alteration are up for consideration for further research since hydrothermal alteration is a crucial factor in the localisation of orogenic gold deposits. (Fanton et al. 2011; Akinlalu 2023; Adetona et al. 2023; Aliyu et al. 2021; kwaghhua et al. 2021).

5.0 CONCLUSION

Comprehensive analysis of both magnetic and radiometric data within Minna sheet 164 was achieved and used to narrow the observe basement structural deformation in terms of faults, fractures and joints to regions of hydrothermal alterations due to observed potassium enrichment or/and thorium deprivation, that could serve as haloes of gold mineralisation. Mathematical control algorithms such as Vertical and Horizontal Derivatives, and 3-D Euler deconvolution were employed to investigate the available structures of interest. The result showcase several lineaments classified as faults and fractures labelled F1 to F8 (for fractures) located at various part of the study area such as within Maikunkele, Shakwatu, Shekwata, Asha, Sarkin- Pawa, Kafin-Koro, Gunu and Fuka. Majority of these lineaments are trending in the NW-SE directions. The total amplitude gradient reveal a basement that has undergone high degree of brittle deformation as a result of tectonic events. The filtered Euler solutions structures in form of dykes, depth of these structures are in the range 0 to 86 meters in the majority.

The radiometric data was was used to obtain K/eTh, K_deviation and F_parameter analysis, a combination of these three produces a ternary image by combining K/eTh (in Blue), K-derivative (in Red) and F-parameter (in Green) as shown in Fig. 10 which shows area of anomalous high hydrothermal altered haloes in white colour and moderate altered hydrothermal holes in (grey-blue) colour. These are areas at the North-Western which falls within **Shakwatu, Shekwata, Gunnu, Shiroro, Shiroro, Gunni Fuka, Minna and Tudun-Fulani.** These regions are intruded by fault-lines labelled F1, F2, F3, F4, and F5 respectively. Those altered zones delineated at the Southern end of the study area are influenced by fault-lines labelled F6, F7, and F8 respectively.
The highest hydrothermal signature correlates with biotite gneiss zones intruded by quartz schist, typical hosts for orogenic gold. From figure 14 regions of High priority are: Shakwatu–Shekwata Minna and Tudun-Fulani shows strong alignment of faults and alteration zones regions of Moderate priority are: Gunu–Fuka while regions of Low priority: South-eastern zones with weak alteration signals. Given ongoing artisanal mining in parts of the study area, findings from this study can support safer and more efficient resource extraction with minimal environmental impact. A super imposed map (figure 14), consisting of the altered zones, structural lineament and location depict a clearer picture of the regions of alteration strike through by lineaments. Summary of these results can be seen on table 2.

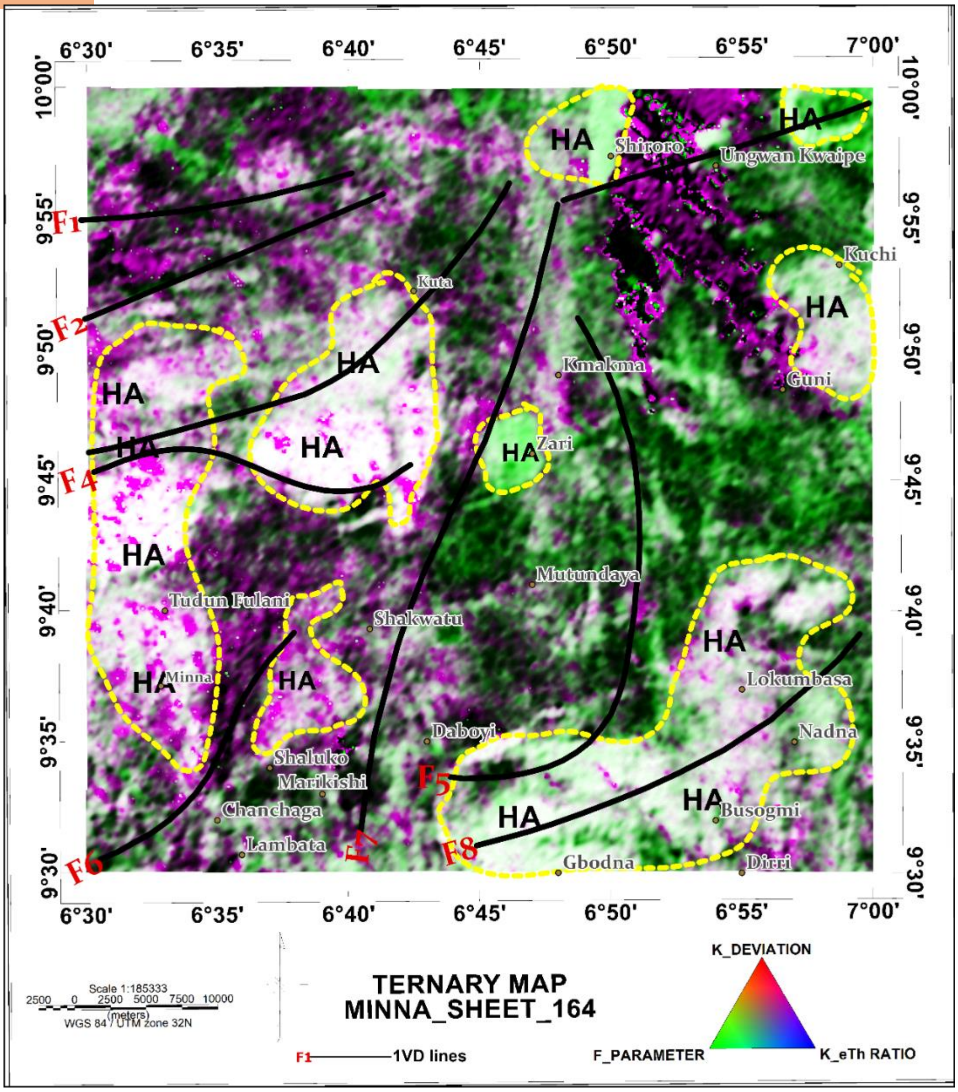

Figure: 14. Super-imposed Altered Zone, Structural lineaments and Location maps

Table 2: summary of probable zones base on degree of alteration

SN	Location	LATITUDE	LONGITUDE	ROCK TYPE	ALTERATION
1	SHIRORO & SARKIN-PAWA	9.60^{o} -- 10.00 ^{o}	9.60^{o} -- 10.00 ^{o}	Schist,Myonite Amphybolites	Fairly
2	UNGRAN-KWAIOE	9.60^{o} -- 10.00 ^{o}	6.55^{o} -- 7.00 ^{o}	Schists	Fairly
3	GUNNI	9.50O -- 9.55 ^{o}	9.60^{o} -- 10.00 ^{o}	Migmatite, Schist	Moderately
4	SHEKWATA	9.45O -- 9.55 O	6.35O -- 6.45 O	Granite, Schist	Highly
5	MINNA & TUDUN-FULANI	9.35^{o} -- 9.50 ^{o}	6.30^{o} -- 6.35 ^{o}	Granite Migmatite And Schist	Highly
6	BUSOGMI & FUKA	9.30^{o} -- 9.45 ^{o}	6.45^{o} -- 6.55^{o}	Porphyritic Granite	Highly
7	SHAKWATU	9.45^{o} -- 9.50^{o}	6.40^{o} -- 6.45^{o}	Granite, Schist	Fairly
8	Gurusu	9.30^{o} -- 9.45^{o}	6.30^{o} -- 6.40^{o}	Schist, Granite &Quartz	Fairly

5.1. RECOMMENDATIONS

The result of this work showed that the gold mineralization in Sheet 164 (Minna) is encouraging, however, complete accounts of the gold and allied potentials of this and similar anomalies in figure 13 would only be confirmed, after further geochemical and mineralogical investigations on samples from the area delineated as most probable gold mineralization. Geochemical and mineralogical investigations of the area should be carried out to reconfirm the geophysical finding of the area

Conflict of Interests: The authors declare no conflict of interest.

REFERENCES

Abd El Nabi, S. H. (2013). Role of γ-ray spectrometry in detecting potassic alteration associated with Um Ba'anib granitic gneiss and metasediments, G. Meatiq area, Central Eastern Desert, Egypt. *Arabian Journal of Geosciences*, *6*, 1249-1261. https://doi.org/10.1007/s12517-011-0378-4

Adams, J. S., & Gasparini, P. (1970). *Methods in Geochemistry and Geophysics.-Gamma-Ray Spectrometry of Rocks*. Elsevier.

Adeleke, A. A., Nemakhavhani, T. W., & Popoola, A. P. I. (2014). Evaluation of the Cyanidation Leaching of Gold in a Waste Rock Ore. *Iran. J. Chem. Chem. Eng. Vol*, *33*(2).

Adetona, A. A., Fidelis, I. K., & Shakarit, B. A. (2023). Interpreting the magnetic signatures and radiometric indicators within Kogi State, Nigeria for economic resources. *Geosystems and Geoenvironment*, *2*(2), 100157. https://doi.org/10.1016/j.geogeo.2022.100157

Agterberg, F. P., & Bonham-Carter, G. F. (1999, October). Logistic regression and weights of evidence modeling in mineral exploration. In *Proceedings of the 28th international symposium on applications of computer in the mineral industry (APCOM), Golden, Colorado* (Vol. 483, p. 490).

Airo, M. L. (2002). Aeromagnetic and aeroradiometric response to hydrothermal alteration. *Surveys in Geophysics*, *23*, 273-302.

Ajibade, A. C., & Wright, J. B. (1989). The Togo-Benin-Nigeria Shield: evidence of crustal aggregation in the Pan-African belt. *Tectonophysics*, *165*(1-4), 125-129.

Akinlalu, A. A. (2023). Radiometric mapping for the identification of hydrothermally altered zones related to Gold mineralization in Ife–Ilesa schist belt, southwestern Nigeria. *Indonesian Journal of Earth Sciences*, *3*(1), A519-A519.

Allen, R. L. (1995). Atlas of Alteration. A Field and Petrographic Guide to Hydrothermal Alteration Minerals. *Geological Association of Canada*, Mineral Division.

Aliyu, S.B., Adetona, A. A., Adewuyi, R. A., Jude, E., Adewumi, T. (2021). Delineating and interpreting the gold veins within Bida and Zungeru Area, Niger State Nigeria, using aeromagnetic and radiometric data. *Pakistan Journal of Geology*. DOI: https://doi.org/10.2478/pjg-2021-0006

An, P., Moon, W. M., & Rencz, A. (1991). Application of fuzzy set theory for integration of geological, geophysical and remote sensing data. *Canadian Journal of Exploration Geophysics*, *27*(1), 1-11.

Augie, A. I., & Ologe, O. (2020). Analysis of Aeromagnetic Data for Coal Deposit Potential over Birnin Kebbi and its Environs Northwestern Nigeria. *Nigerian Journal of Science and Environment*, *18*(1), 145.

Bierlein, F. P., Fuller, T., Stüwe, K., Arne, D. C., & Keays, R. R. (1998). Wallrock alteration associated with turbidite-hosted gold deposits. Examples from the Palaeozoic Lachlan Fold Belt in central Victoria, Australia. *Ore Geology Reviews*, *13*(1-5), 345-380.

Cunha, L. O., Dutra, A. C., & Costa, A. B. (2017). Use of radiogenic heat for demarcation of hydrothermal alteration zones in the Pernambuco-Brazil. *Journal of Applied Geophysics*, *145*, 111-123.

Danbatta, U. A. (2008). Precambrian crystal development in the northerwestern part of Zuru schist belt, northwestern Nigeria. *Journal of Mining and Geology*, *44*(1), 45-56.

Danbatta, U. A. (2005). Precambrian crustal development of the northwestern part of Zuru schist belt, NW Nigeria. In *A paper presented at the 41st Annual Conference of Nigerian Mining, and Geos. Soc.(NMGS).*

Danjumma, S. G., Senchi, D. B., Sale, L., Mohammed, A., & Tudu, A. M. B. (2019). Identification of Mineral Deposits in Garin Awwal Mining Site, Kebbi State, North-Western Nigeria. *environment*, *6*(6).

de Quadros, T. F., Koppe, J. C., Strieder, A. J., & Costa, J. F. C. (2003). Gamma-ray data processing and integration for lode-Au deposits exploration. *Natural Resources Research*, *12*, 57-65.

Dickson, B. L., & Scott, K. M. (1997). Interpretation of aerial gamma-ray surveys-adding the geochemical factors. *AGSO Journal of Australian Geology and Geophysics*, *17*.

Efimov, A. V. (1978). Multiplikativnyj pokazatel dlja vydelenija endogennych rud poaerogamma-spektrometriceskim dannym. *Metody rudnoj geofiziki. Leningrad, Naucno-proizvodstvennoje objedinenie geofizika.*

Eleraki, M., Ghieth, B., Abd-El Rahman, N., & Zamzam, S. (2017). Hydrothermal zones detection using airborne magnetic and gamma ray spectrometric data of mafic/ultramafic rocks at Gabal El-Rubshi area, Central Eastern Desert (CED), Egypt. *Advances in Natural and Applied Sciences*, *11*(9), 182-197.

Fanton, G., Martinez, M. P., & Gimenez, M. E. (2011, August). AeroGammaspectrometry for Lode-Au Deposits Exploration In Western Pampean Ranges-Argentine. In *12th International Congress of the Brazilian Geophysical Society & EXPOGEF, Rio de Janeiro, Brazil, 15–18 August 2011* (pp. 1124-1129). Society of Exploration Geophysicists and Brazilian Geophysical Society.

Garba, I. (2000). Gold prospect of the Nigerian Pan-African terrain of West Africa. *J. Min. Geol*, *36*(2), 123-126.

Garba, I. (2002). Late Pan-African tectonics and origin of gold mineralization and rare-metal pegmatities in the Kushaka schist belt, northwestern Nigeria. *Journal of mining and geology*, *38*(1), 1-12. https: //doi.org/10.4314/jmg. v38i1 .18768

Garba, I. (2003). Geochemical characteristics of mesothermal gold mineralisation in the Pan-African (600±150 Ma) basement of Nigeria. *Applied Earth Science*, *112*(3), 319-325.

Galbraith, J. H., & Saunders, D. F. (1983). Rock classification by characteristics of aerial gamma-ray measurements. *Journal of Geochemical Exploration*, *18*(1), 49-73.

Geosoft (2009) Grav/Mag interpretation. Montaj extension developed by Geosoft (Electronic version); Oasis Montaj Data Processing Analysis (DPA) system for Earth sciences applications. *Euro Technologies.*

Jambon, J. L. (2007). Wall Rock Alteration, Geological Survey of Canada, Ottawa

Kwaghhua, F. I., Adetona, A. A., Aliyu, S. B. (2021). Interpretation of major structures within the basement region of Benue-Niger confluence from Aeromagnetic and Radiometric data Kogi state Nigeria. *Geological Behavior (GBR)* 2021. DOI: 10.26480/gbr.01.2021.17.22

Li, X. (2008). Magnetic reduction-to-the-pole at low latitudes: Observations and considerations. *The leading edge*, *27*(8), 990-1002.

Maden, N., & Akaryalı, E. (2015). Gamma ray spectrometry for recognition of hydrothermal alteration zones related to a low sulfidation epithermal gold mineralization (eastern Pontides, NE Türkiye). *Journal of Applied Geophysics*, *122*, 74-85.

Ministry Of Mines and Steel Development (2010). Gold Deposits Exploration in Nigeria. (n.d). Retrieved from http://www.mmsd.gov.ng/gold/ 2010.

Olugbenga, T. T., & Augie, A. I. (2020). Estimation of crustal thickness within the Sokoto Basin, North-Western Nigeria using bouguer gravity anomaly data. *International Journal of Geological and Environmental Engineering*, *14*(9), 247-252.

Pires, A. C. B. (1995). Identificação geofisica de áreas de alteração hidrotermal, Crixás-Guarinos, Goiás. *Brazilian Journal of Geology*, *25*(1), 61-68.

Quadros, T. D. (2000). *Integraçoã de dados para pesquisa mineral de ouro em ambiente SIG na Ilha Cristalina de Rivera, Uruguai* (Doctoral dissertation, Tese de Doutoramento, PPGEM, Escola de Engenharia: Universidade Federal do Rio Grande do Sul, PortoAlegre, 260p).

Reid, A. B., Allsop, J. M., Granser, H., Millett, A. T., & Somerton, I. W. (1990). Magnetic interpretation in three dimensions using Euler deconvolution. *Geophysics*, *55*(1), 80-91.

Sanusi, S. O., & Amigun, J. O. (2020a). Structural and hydrothermal alteration mapping related to orogenic gold mineralization in part of Kushaka schist belt, North-central Nigeria, using airborne magnetic and gamma-ray spectrometry data. *SN Applied Sciences*, *2*, 1-26.

Sanusi, S. O., & Amigun, J. O. (2020b). Logistic-based translation of orogenic gold forming processes into mappable exploration criteria for fuzzy logic mineral exploration targeting in the Kushaka schist belt, North-central Nigeria. *Natural Resources Research*, *29*(6), 3505-3526.

Sani, D. G., Senchi, D. B., Sale, L., Mohammed, A., & Tudu, A. M. B. (2019). Identification of Mineral Deposits in Garin Awwal Mining Site, Kebbi State, North-Western Nigeria. *environment*, *6*(6).

Saunders, D. F., Terry, S. A., & Thompson, C. K. (1987). Test of national uranium resource evaluation gamma-ray spectral data in petroleum reconnaissance. *Geophysics*, *52*(11), 1547-1556.

Thompson, D. T. (1982). EULDPH: A new technique for making computer-assisted depth estimates from magnetic data. *Geophysics*, *47*(1), 31-37.

Yannah, M., Suh, C. E., & Mboudou, M. G. M. (2015). Quartz veins characteristics and Au mineralization within the Batouri Au District, East Cameroon. *Sci. Res*, *3*(4), 137149. https://doi.org/10.11648/j.sr.20150304